Polymer Chemistry

Accepted Manuscript

This article can be cited before page numbers have been issued, to do this please use: G. Yu, R. Zhao, D. Wu, F. Zhang, L. Shao, J. Zhou, J. Yang, G. Tang, X. S. Chen and F. Huang, *Polym. Chem.*, 2016, DOI: 10.1039/C6PY01402J.

ROYAL SOCIETY OF CHEMISTRY

www.rsc.org/polymers

View Article Online
DOI: 10.1039/C6PY01402J

Polymer Chemistry

ARTICLE

Pillar[5]arene-based amphiphilic supramolecular brush copolymer: fabrication, controllable self-assembly and application in self-imaging targeted drug delivery†

Received 00th January 20xx,
Accepted 00th January 20xx

DOI: 10.1039/x0xx00000x

www.rsc.org/

Guocan Yu,[a,c,‖] Run Zhao,[a,‖] Dan Wu,[b,‖] Fuwu Zhang[c] Li Shao,[a] Jiong Zhou,[a] Jie Yang,[a] Guping Tang,[b] Xiaoyuan Chen,[c,*] and Feihe Huang[a,*]

Supramolecular brush copolymers have attracted continuing interest due to their unusual architectures, fascinating properties, and potential applications in many fields involving smart stimuli-responsive drug delivery systems. Herein, the first pillararene-based amphiphilic supramolecular brush copolymer (**P5-PEG-Biotin⊃PTPE**) was constructed on the basis of the host–guest molecular recognition between a water-soluble pillar[5]arene (**P5**) and a viologen salt (**M**). **P5-PEG-Biotin⊃PTPE** self-assembled into supramolecular nanoparticles (**SNPs**), which were utilized as a self-imaging drug delivery vehicle by taking advantage of the aggregation-induced emission (AIE) effect. Encapsulation of anticancer drug doxorubicin (DOX) caused deactivation of the fluorescences of both the tetraphenylethene (TPE) and DOX chromophores due to the energy transfer relay (ETR) effect, mediated by Förster resonance energy transfer (FRET) and aggregation-caused quenching (ACQ). The release of loaded DOX molecules can be triggered by low pH and reductase, recovering the "silenced" fluorescence caused by the interruption of the ETR effect, achieving *in situ* visualization of the drug release process by observing the location and magnitude of the energy transfer-dependent fluorescence variation. The biotin ligands on the surfaces of the DOX-loaded **SNPs** act as targeting agents to deliver DOX preferentially to cancer cells over-expressing biotin receptor. *In vitro* studies demonstrated that the loading of DOX by this supramolecular nanomaterial exhibited selective cytotoxicity towards cancer cells over normal cells. The potency of this sophisticated supramolecular drug delivery system in cancer therapy was further evaluated in HeLa tumor-bearing mice. *In vivo* experiments confirmed that the DOX-loaded **SNPs** possess excellent antitumor efficacy with negligible systemic toxicity.

Introduction

Brush copolymers, a class of branched or graft copolymers with polymeric side-chains attached to a linear backbone, have become an exciting and active area of research in polymer science and engineering.[1] Over the past decades, these polymer brushes have been widely employed in many fields involving drug delivery, biosensing, and photonic crystals, because of their unusual architectures and fascinating properties.[2] Generally, there are three synthetic methods for the synthesis of polymer brushes, namely, "grafting through" (polymerization of macromonomers), "grafting to" (attachment of the side chains to the backbone), and "grafting from" (grafting the side chains from the backbone).[3] However, most of the reported polymer brushes are conventional covalent polymers, requiring painstaking syntheses and post modifications.[4] Additionally, the macromonomer conversion, the degree of polymerization, grafting density, and polydispersity are hardly controlled by these conventional synthetic strategies. Furthermore, it is not easy to realize controlled disassembly due to covalent connections between blocks in polymer brushes that lack stimuli-responsiveness, greatly limiting their applications in various fields.

Supramolecular brush copolymers (SBPs) fabricated from simpler molecular building blocks through non-covalent interactions exhibit tremendous advantages, since supramolecular approaches have potential to overcome some drawbacks of 'covalent' polymer brushes syntheses,[5] and bring about some exploitable stimuli-responsive properties for the resultant SBPs.[6] For example, SBPs possess incomparable advantages in biomedical applications owing to their distinctive topological structures and relatively low critical aggregation concentrations.[7] On the other hand, a large amount of drug can be loaded into the self-assemblies formed from SBPs due to their compact architectures, providing a sufficient drug concentration in the active sites. More importantly, functional nanoparticles (NPs) self-assembled from SBPs can be specifically internalized by cancer cells and the loaded drug can be released triggered by intracellular stimuli, leading to higher anticancer efficacy with reduced side effects.[8]

[a] *State Key Laboratory of Chemical Engineering, Center for Chemistry of High-Performance & Novel Materials, Department of Chemistry, Zhejiang University, Hangzhou 310027, P. R. China. Fax and Tel: +86-571-8795-3189 Email address: fhuang@zju.edu.cn.*
[b] *Department of Chemistry, Institute of Chemical Biology and Pharmaceutical Chemistry, Zhejiang University, Hangzhou 310027, P. R. China.*
[c] *Laboratory of Molecular Imaging and Nanomedicine, National Institute of Biomedical Imaging and Bioengineering, National Institutes of Health, Bethesda, Maryland 20892, United States. Email address: chenx5@mail.nih.gov.*

† Electronic Supplementary Information (ESI) available: Experimental details, NMR spectra, and other materials. See DOI: 10.1039/b000000x/

View Article Online
DOI: 10.1039/C6PY01402J

Various non-covalent forces, such as hydrogen bonding, metal-coordination, hydrophobic interactions, π–π interactions, charge-transfer interactions, and van der Waals interactions can be employed to construct SBPs. Among them, host–guest interactions have gained much attention due to their abundant stimuli-responsiveness.[9] However, rare examples have been reported using host–guest recognition motifs to fabricate SBPs. Compared with other macrocyclic hosts, such as crown ethers, cyclodextrins, calixarenes, and cucurbiturils,[10] their unique symmetrical structure and easy modification endow pillar[*n*]arenes with superior properties in host–guest recognition,[11] which provide opportunities to construct smart stimuli-responsive SBPs.

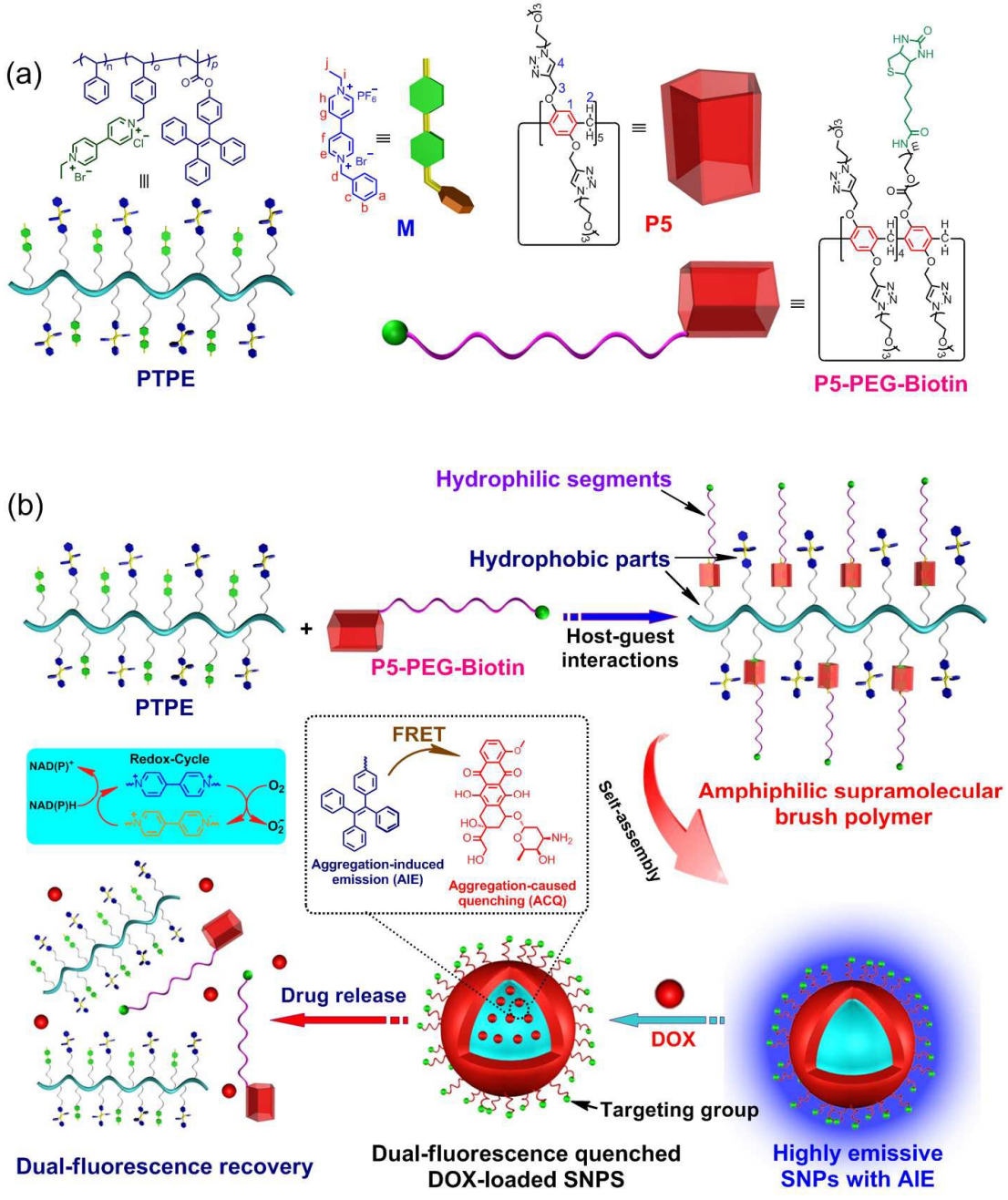

Scheme 1. (a) Chemical structures and cartoon representations of **M**, **P5**, **P5-PEG-Biotin** and **PTPE**. (b) Schematic illustration of the formation of **SNPs** self-assembled from the amphiphilic supramolecular brush copolymer **P5-PEG-Biotin⊃PTPE** and their use as drug delivery vehicles.

Before applying SBPs in drug delivery systems (DDSs), there exists another issue to be solved. Traditional DDSs are typically "one trick ponies", and their sole role is to deliver drugs into cancer cells. These DDSs constructed from common biocompatible polymers, such as poly(glycolic acid) (PGA), poly($_{D,L}$-lactic acid) (PLA), poly($_{D,L}$-lactic-coglycolic acid) (PLGA), and poly(ethylene glycol) (PEG), are invisible and difficult to trace after they enter the cells and release the drugs. Therefore, it is desirable to develop

View Article Online
DOI: 10.1039/C6PY01402J

"visible" nano-vehicles to track their distribution *in vitro* and *in vivo* during drug delivery. Generally, covalent modifications and non-covalent encapsulation of fluorescent dyes are the most commonly employed methods to trace the delivery of DDSs. However, these methods have drawbacks that limit their clinical applications: i) the fluorophores grafted onto the polymeric vehicles may be hydrolyzed and detached from the DDSs during the phagocytic process, so that the subcellular location marked by the fluorescent dye may not represent their actual position; ii) the aggregation caused quenching (ACQ) effect always take place for the traditional fluorophores when they are assembled into NPs; iii) the fluorescence of the traditional fluorophores is easily photo-quenched; iv) the fluorophores loaded through non-covalent encapsulation leak from the DDSs during the delivery process, making the obtained fluorescence signal confusing. Therefore, searching for novel self-imaging drug carriers with "turn on" fluorescence that is activated upon assembly is highly desirable.

Herein, we develop a novel pillar[5]arene-based host–guest molecular recognition motif between a water-soluble pillar[5]arene (**P5**) and a 4,4'-bipyridinium derivative (**M**) in water, mainly driven by charge transfer and hydrophobic interactions. The first pillar[5]arene-based amphiphilic SBP (**P5-PEG-Biotin⊃PTPE**) was successfully fabricated on the basis of this recognition motif by using **PTPE** and **P5-PEG-Biotin** as building blocks (Scheme 1). The core-shell structured NPs formed by **P5-PEG-Biotin⊃PTPE** were used as a DDS to encapsulate the anticancer drug doxorubicin (DOX), forming a dual-fluorescence quenched Förster resonance energy transfer (FRET) system, wherein the tetraphenylethene (TPE) groups act as donor fluorophores and the DOX units act as the acceptors.[12] Under the action of intracellular reductase and low pH environment, the loaded drug molecules are released. As a consequence, the energy transfer relay (ETR) effect between DOX and TPE is interrupted,[13] and the "silenced" fluorescence "wakes up", achieving *in situ* visualization of the drug release via the location and magnitude of the energy transfer-dependent fluorescence variation (Scheme 1). The biotin ligands on the surfaces of the supramolecular nanoparticles (**SNPs**) act as targeting agents to deliver DOX preferentially to cancer cells over-expressing biotin receptors. *In vitro* investigations revealed the cancer cell specific therapeutic efficacy of the DOX-loaded **SNPs**, while their cytotoxicity towards normal cell was greatly reduced. The potency of this sophisticated supramolecular DDS in cancer therapy was evaluated in HeLa tumor-bearing mice. *In vivo* experiments confirmed DOX-loaded **SNPs** possess excellent antitumor ability with negligible systemic toxicity, which was attributed to targeting ability and the enhanced permeability and retention (EPR) effect.

Results and discussions

The host−guest complexation between model host **P5** and model guest **M** (Fig. 1) was first studied by ^{1}H NMR spectroscopy. Compared with free **M**, the resonance peaks related to protons on **M** exhibited slight upfield shifts in the presence of **P5** (Fig. 1, spectra b and c) because these protons were located in the cavity of **P5** and shielded by the electron-rich cyclic structure after the formation of an inclusion complex between **P5** and **M**.[14] On the other hand, a broadening effect was observed for the peaks corresponding to protons $H_{d–g}$ and H_j due to the complexation dynamics. Notably, negligible chemical shift changes were observed for the signals related to protons $H_{a–c}$, demonstrating that these protons were outside of the electron-rich cavity. Furthermore, the signals related to the protons on **P5** also exhibited slight chemical shift changes caused by the host−guest complexation between **P5** and **M**. 2D NOESY NMR spectroscopy was carried out to investigate the relative positions of the components in the host−guest inclusion complex (Fig. S4). Strong nuclear Overhauser effect (NOE) correlations were observed between the signals related to the protons on **M** and the protons (H_1 and H_4) of **P5**, suggesting that **M** was threaded into the cavity of the pillararene moiety, in agreement with the results obtained from ^{1}H NMR investigations.

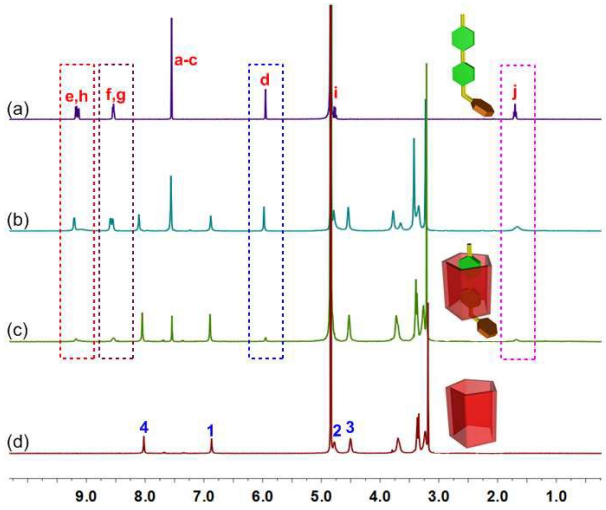

Fig. 1 Partial ^{1}H NMR spectra (400 MHz, D_2O, 295 K): (a) **M** (1.00 mM); (b) **P5** (1.00 mM) and **M** (3.00 mM); (c) **P5** (1.00 mM) and **M** (1.00 mM); (d) **P5** (1.00 mM). (e) 2D NOESY NMR spectrum (500 MHz, D_2O, 295 K) of **P5** (10.0 mM) and **M** (30.0 mM).

Fluorescence titrations were carried out to estimate the association constant for the complexation between **P5** and **M**. As shown in Fig. S5, significant quenching of fluorescence intensity was found upon gradual addition of **M** to a solution of **P5** due to the host−guest complexation. A mole ratio plot on the basis of the fluorescence titration experiments demonstrated that the complex between **P5** and **M** had 1:1 stoichiometry (Fig. S6). The association constant (K_a) was calculated to be (2.50 ± 0.16) × 10^4 M^{-1} using a non-linear curve-fitting method (Fig. S7). The driving forces for the formation of **P5⊃M** were attributed to the cooperativity of hydrophobic interactions and charge transfer interactions between electron-rich **P5** and electron-poor **M**.[111] The formation of 1:1 host–guest complex between **P5** and **M** was further confirmed by a low-resolution electrospray ionization mass spectroscopy peak at *m*/*z* 1580.5 (Fig. S11), corresponding to $[\mathbf{P5}\supset\mathbf{M} - Br - PF_6]^{2+}$.

View Article Online
DOI: 10.1039/C6PY01402J

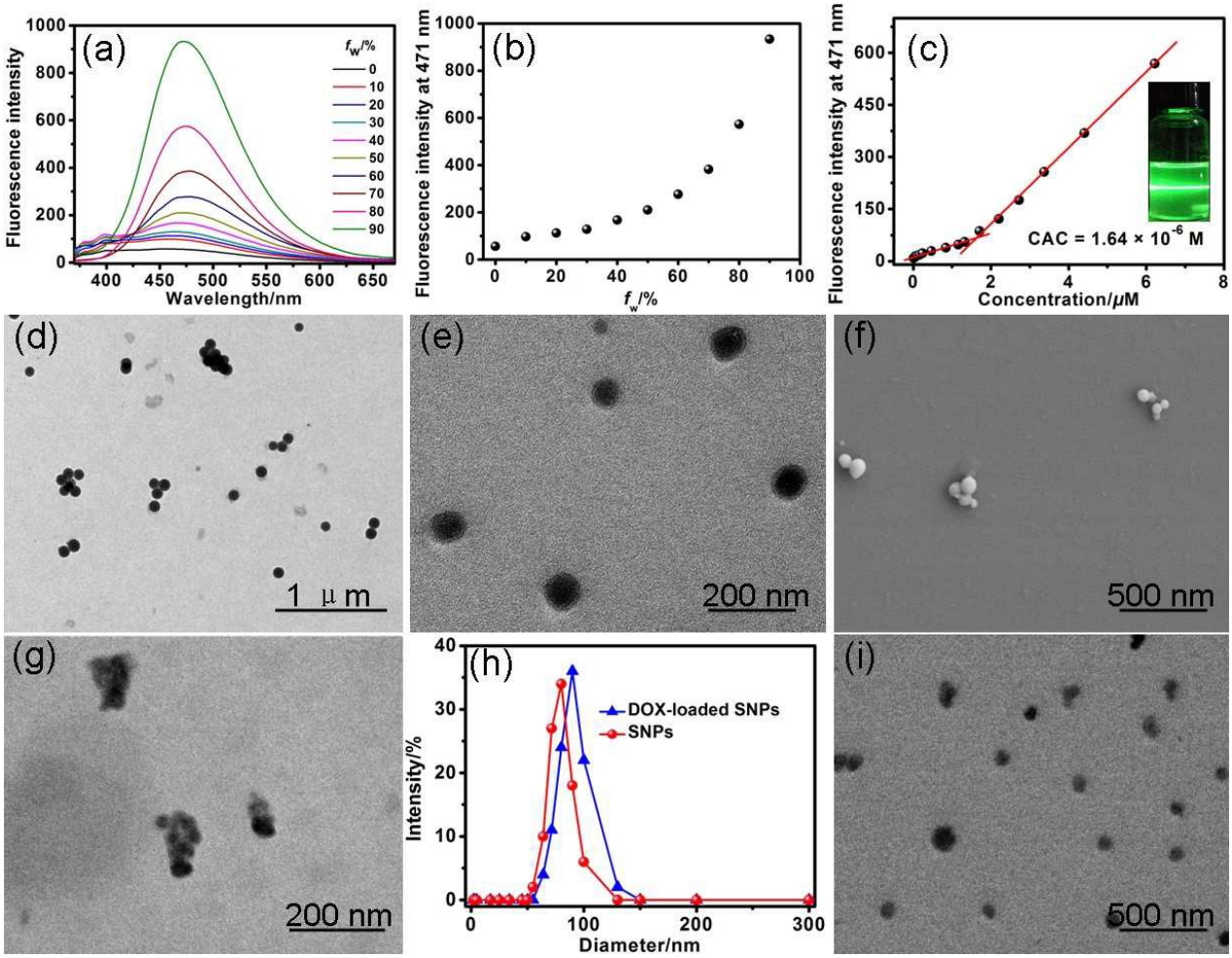

Fig. 2 (a) Fluorescence spectra of **P5-PEG-Biotin⊃PTPE** in mixtures of THF and water with different f_w values. (b) Plot of the emission intensity at 471 nm *vs*. f_w of the aqueous mixtures. The concentration of **P5-PEG-Biotin⊃PTPE** was 2.00 mg/mL. (c) Plot of the emission intensity at 471 nm *vs*. the concentration of **P5-PEG-Biotin⊃PTPE**. (d,e) TEM and (f) SEM images of the **SNPs** self-assembled from **P5-PEG-Biotin⊃PTPE**. (g) TEM image of the **SNPs** in the presence of $Na_2S_2O_4$ (0.1 mg/mL). (h) DLS size distributions of **SNPs** and DOX-loaded **SNPs**. (i) TEM images of DOX-loaded **SNPs**.

By utilizing the host−guest recognition motif based on **P5** and **M**, an amphiphilic SBP (**P5-PEG-Biotin⊃PTPE**) was constructed, of which the backbone and TPE units of **PTPE** acted as the hydrophobic parts and the PEG chains worked as the hydrophilic sections. Upon formation of **P5-PEG-Biotin⊃PTPE**, the AIE property of **PTPE** was maintained.[15] It had faint fluorescence intensity when dissolved in THF, but fluoresced intensively when the volume fraction of water (f_w) value increased (Fig. 2, a and b). The dependence of the solution fluorescence *vs*. the solution concentration was used to determine the critical aggregation concentration (CAC). When the concentration was lower than the CAC, the fluorescence was poor, while the fluorescence intensity rose abruptly as the concentration was higher than the CAC value, caused by the AIE effect due to the self-assembly of **P5-PEG-Biotin⊃PTPE** (Fig. 2c). By plotting the fluorescence intensity changes at 471 nm *vs*. the concentration, the CAC value of **P5-PEG-Biotin⊃PTPE** was measured to be 1.64 × 10^{-6} M (based on the concentration of **PTPE**), which was much higher than that of **PTPE** by a factor of *ca*. 50 (Fig. S12), arising from the introduction of hydrophilic PEG segments through host−guest complexation. The Tyndall effect was observed when the concentration of **P5-PEG-Biotin⊃PTPE** was higher than its CAC value, indicating the existence of nanoaggregates in aqueous solution (Fig. 2c). The morphology and size of the self-assemblies were fully investigated by transmission electron microscopy (TEM), scanning electron microscopy (SEM), and dynamic light scattering (DLS) studies. As shown in Fig. 2d, NPs diameters about 80 nm were observed in TEM images, in agreement with the result obtained from the DLS measurement showing an average size of 73.9 nm (Fig. 2h). SEM provided further convincing evidence for the formation of supramolecular NPs (**SNPs**) self-assembled from **P5-PEG-Biotin⊃PTPE** (Fig. 2f).

From previous work, we knew that viologens (**PQ**) could be reduced into the corresponding cationic radical state by the

View Article Online
DOI: 10.1039/C6PY01402J

intracellular reductase, such as NAD(P)H.[16] Fluorescence titration experiment demonstrated that the K_a value between pillar[5]arene and $\mathbf{M}^{\bullet+}$ decreased to (6.67 ± 0.45) × 10^2 M^{-1} (Fig. S8–S10), because the charge-transfer interactions became weaker when the dicationic **PQ** was reduced into the radical cationic state. Accompanied by the reduction of **PQ**, the binding affinity between pillar[5]arene and **PQ** decreased significantly, resulting in the disassembly of the NPs. TEM revealed that the **SNPs** dissociated into irregular aggregates in the presence of 0.1 mg/mL $Na_2S_2O_4$ (Fig. 2g).

The hydrophobic core of the NPs could be employed to encapsulate the hydrophobic anticancer drug DOX. Moreover, π-π interactions between the aromatic rings on **PTPE** and DOX were favorable to enhance the loading efficiency. The drug loading efficiency was estimated to be 26.7% by weight. After encapsulation of DOX, a negligible change in morphology of the NPs was observed, with only a slight increase in the mean diameter (Fig. 2i). The average diameter of the NPs changed from 73.9 nm to 86.4 nm after loading DOX (Fig. 2h).

In an effort to precisely characterize the nature and location of stimuli-responsive drug release, DDSs with intrinsic fluorescence capable of responding to the specific microenvironments need to be developed, since most of the anticancer drugs such as cisplatin, gemcitabine, and paclitaxel are intrinsically non-fluorescent or weakly fluorescent.[17] Self-imaging DDSs in which dynamic energy-transfer processes occur between the drug and the carrier, such as FRET, are attracting great attention.[18] When the drug is released in specific environments within living cells, these energy transfers are broken, resulting in a variation in the fluorescent signal, which was used to track the process of translocation, drug release, and excretion of the nanomedicine. Fig. 3a shows a well overlap between the emission spectrum of **PTPE** and the absorption spectrum of DOX, indicating that **PTPE** could act as a fluorescent donor for DOX. The fluorescent spectra of the NPs in the presence of DOX were measured to confirm the FRET phenomenon (Fig. 3b).[12a] The fluorescence intensity at 470 nm ascribed to the characteristic emission of **PTPE** decreased gradually upon addition of DOX, indicating that the AIE behavior disappeared by its introduction into **SNPs**, due to FRET from the TPE-based fluorogens to DOX.[13] Time-resolved spectroscopy was also utilized to study the photophysical behavior of **SNPs** in the absence and presence of DOX (Fig. 3c and d). The weighted mean lifetime (τ) was calculated to be 4.38 ns for **SNPs**. However, the τ value decreased to 2.31 ns in the presence of DOX. From these analyses, the efficiency of energy transfer (Φ_T) of this system was calculated to be 47.3% according to the equation: $\Phi_T = 1-\tau_D/\tau_{DA}$, where τ_D and τ_{DA} represented the lifetimes of the fluorescent donor in the absence and presence of fluorescent acceptor (DOX), respectively. These studies confirmed the successful achievement of FRET, because the TPE groups and DOX coexisted in the hydrophobic core of the NPs and the intermolecular distance between TPE and DOX was close. On the other hand, the ACQ effect of DOX molecules self-quenched their fluorescence intensity by "π-π stacking" of their rigid planar aromatic rings. Moreover, blue shifts were monitored for the maximum emission of **SNPs** accompanied by the addition of DOX, suggesting that the addition of DOX made **SNPs** less aggregated as demonstrated by TEM (Fig. 2i).[12a] Thus, a dual-fluorescence-quenched supramolecular system was obtained through the ETR effect.

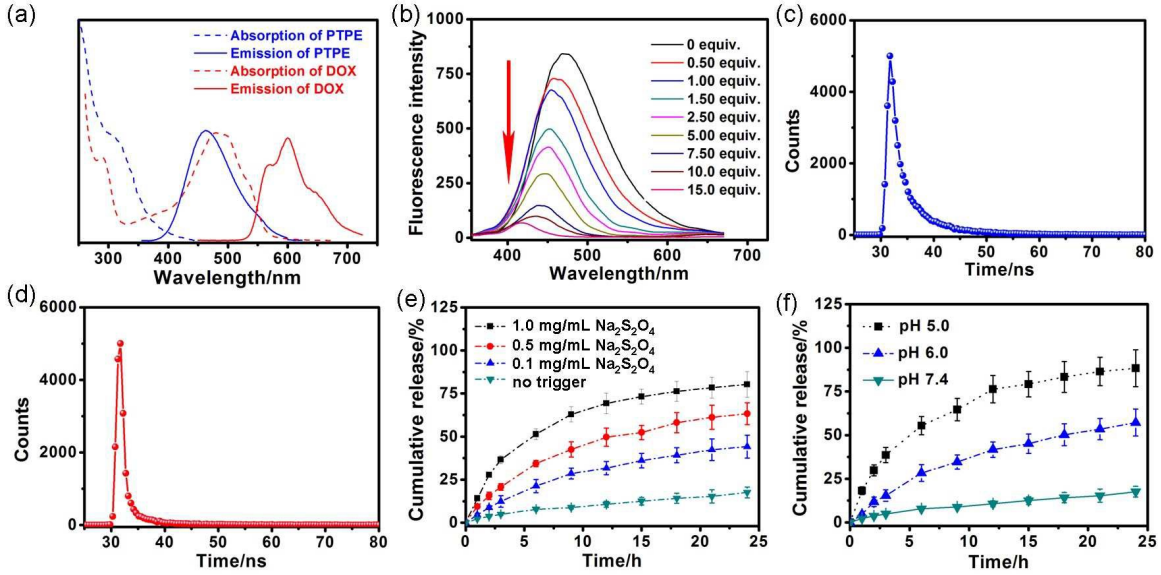

Fig. 3 (a) Absorption and fluorescence emission spectra of **P5-PEG-Biotin⊃PTPE** and DOX. (b) Fluorescence spectra of **SNPs** self-assembled from **P5-PEG-Biotin⊃PTPE** in the presence of different amounts of DOX. Fluorescence lifetimes of (c) SNPS and (d) DOX-loaded **SNPs**. (e) Drug release profiles of DOX-loaded **SNPs** with or without different concentrations of the reducing agent. (f) Drug release profiles of DOX-loaded **SNPs** at different solution pH.

The reduction-triggered disassembly of **SNPs** was used to release the loaded anticancer drug. The release profile was evaluated by dialysis in the absence or presence of different concentrations of $Na_2S_2O_4$ (Fig. 3e). In the absence of $Na_2S_2O_4$, only 17.1% DOX was

View Article Online
DOI: 10.1039/C6PY01402J

released within 24 h. In the presence of 0.1, 0.5, and 1.0 mg/mL $Na_2S_2O_4$, 43.7%, 62.8% and 80.5% DOX were released, respectively, in the same time scale, resulting from reduction-triggered disassembly of the DOX-loaded **SNPs**. The neutral DOX encapsulated in the core of the NPs is protonated into the cationic state in the acidic intracellular environment, speeding up its release. The release behavior of DOX from DOX-loaded **SNPs** was also carried out at pH 7.4, 6.0, and 5.0, respectively, mimicking the pH gradient from blood circulation to the endo/lysosomal compartments. As shown in Fig. 3f, the DOX release profile was clearly pH-dependent, 56.9% of DOX was released from DOX-loaded **SNPs** after 24 h at pH 6.0 and 89.1% at pH 5.0, respectively. As indicated by spectra shown in Fig. S14 and S15, the fluorescence intensities of DOX and **PTPE** recovered effectively once DOX was released, because the ETR effect between **PTPE** and DOX was interrupted. By virtue of the energy transfer between TPE and DOX, *in situ* visualization of the drug release can be achieved by observing the location and magnitude of the energy transfer-dependent fluorescence variation.

The biotin groups on the surfaces of **SNPs** acted as targeting agents, endowing the resultant NPs with the ability to specifically deliver DOX to biotin receptor over-expressing cancer cells, thus minimizing side effects of the drug towards normal tissues.[19] Before applying **SNPs** as drug delivery vehicles, the biocompatibility of the blank **SNPs** was evaluated by a 3-(4′,5′-dimethylthiazol-2′-yl)-2,5-diphenyl tetrazolium bromide (MTT) assay on HeLa and HEK293 cells. Negligible changes were observed in relative cell viability with concentrations of **P5-PEG-Biotin⊃PTPE** ranging from 10 to 500 μg/mL (Fig. 4d), demonstrating excellent biocompatibility of this supramolecular nanomaterial.

The internalization and drug release behavior of the DOX-loaded **SNPs** were further studied by confocal microscopy. HeLa and HEK293 cell lines were used as biotin receptor over-expressing cancer cells and biotin receptor deficient normal cells, respectively. As shown in Fig. 4a, blue fluorescence arising from **PTPE** and red fluorescence related to DOX were observed in the cytoplasm after 15 min treatment, and the fluorescence intensity increased with the incubation time, indicating that DOX was successfully released in a time-dependent manner. Upon incubation with DOX-loaded **SNPs** for 1 h, the subcellular distributions of TPE and DOX remained nearly unchanged compared with the case for 15 min, while the corresponding fluorescence intensity increased significantly. After incubating the HeLa cells with DOX-loaded **SNPs** for 2 h, the fluorescences of TPE and DOX became much brighter, and a large amount of DOX entered the nucleus. By extending the culture time to 4 h, the fluorescence of DOX was mostly localized in the nucleus. It should be noted that the "blue" fluorescence stayed in the cytoplasm and no TPE signal was observed in the nucleus. This phenomenon suggested that **PTPE** delivered DOX into the cells and stayed in the cytoplasm after release of the payload, hardly affecting the anticancer effect of the drug.

In contrast, HEK293 cells showed weak fluorescence signals under the same experimental condition (Fig. 4b), confirming that the biotin groups on the surfaces of DOX-loaded **SNPs** were favorable for delivery of DOX-loaded **SNPs** to cancerous HeLa cells through receptor-mediated endocytosis. We hypothesized that the DOX-loaded **SNPs** were generally internalized by endocytosis, and were translocated into endo/lysosomes. On account of the acidic pH inside the endo/lysosomes, the neutral DOX was protonated into the cationic state, resulting in its release from hydrophobic cores of DOX-loaded **SNPs**. Additionally, the **PQ** groups grafted on the polymer backbone were reduced into the radical cationic state by reductase. The host−guest interactions were weakened, resulting in the disassembly of the DOX-loaded **SNPs**, which accelerated the release of DOX. As a consequence, the ETR effect between **PTPE** and DOX was interrupted, the "silenced" fluorescence "woke up", and the dual-fluorescence quenched system transformed into dual-fluorescence emissive system.

The amount of DOX-loaded **SNPs** internalized by HeLa and HEK293 cells was quantified by flow cytometry investigations. From Fig. 4c, we knew that the mean fluorescence intensity (MFI) of HeLa cells was much higher than that of HEK293 cells under the same conditions, indicating HeLa cells had a faster uptake rate and higher intracellular accumulation of DOX-loaded **SNPs**. For example, HeLa cells ingested about 3 times the amount of DOX-loaded **SNPs** than the HEK293 cells (mean fluorescent intensity of 36.7 *vs* 11.2 a.u.) after incubation for 2 h. Furthermore, pre-treatment with free biotin effectively blocked the biotin receptors, which provided convincing evidence for the targeting ability of DOX-loaded **SNPs**. As shown in Fig. 4a, the pre-treatment with biotin (100 μM) for 0.5 h resulted in the decrease in the MFI value from 36.7 to 15.2 for HeLa cells, confirming significant inhibition of the cellular uptake of DOX-loaded **SNPs**. However, a slight change in the cellular uptake of DOX-loaded **SNPs** was found for HEK293 cells by pre-treating with free biotin, further confirming biotin-receptor interaction between the DOX-loaded **SNPs** and the HeLa cells. These experiments demonstrated that the biotin groups attached on the surfaces of DOX-loaded **SNPs** significantly enhanced the specific targeting ability of DOX-loaded **SNPs** towards biotin receptor over-expressing cancer cells.

The *in vitro* anticancer efficacy of DOX-loaded **SNPs** was evaluated by a MTT assay, wherein the cells treated with free DOX·HCl were used as the control (Fig. 4, e and f). Significant growth inhibition was observed for both HeLa and HEK293 cells incubated with either DOX-loaded **SNPs** or free DOX·HCl at a high DOX concentration, demonstrating that the efficacy of the anticancer drug was maintained effectively after encapsulation by **SNPs**. Compared with free DOX·HCl, the relative cell viability of the cells incubated with DOX-loaded **SNPs** was slightly higher, because higher amount of free DOX·HCl was uptaken by the cells through diffusion. It should be emphasized that DOX-loaded **SNPs** exhibited markedly higher cytotoxicity towards HeLa cells than HEK293 cells at the same concentration of the drug, which was in line with the internalization and drug release studies. The reason was that the existence of biotin groups was favorable to enhance the uptake of DOX-loaded **SNPs** by HeLa cells, thus reducing the toxicity to normal cells. Pre-treatment with free biotin effectively reduced the cytotoxicity of DOX-loaded **SNPs** towards HeLa cells, while the decrease in cytotoxicity against HEK293 cells was much less by pre-treatment with biotin. This phenomenon further demonstrated the DOX-loaded **SNPs** possessed the ability to preferentially deliver the anticancer drug to biotin receptor over-expressing cancer cells.

View Article Online
DOI: 10.1039/C6PY01402J

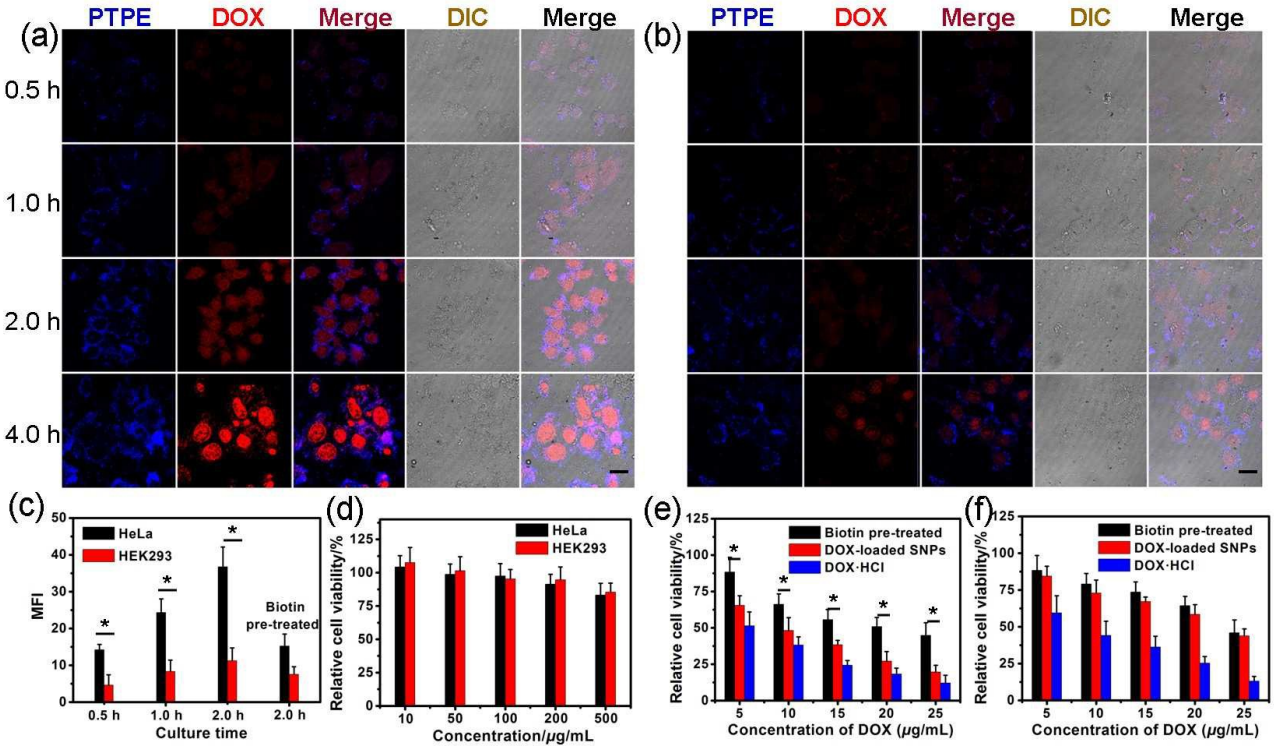

Fig. 4 CLSM images of the (a) HeLa and (b) HEK293 cells incubated with DOX-loaded **SNPs** for different time periods. Scale bars = 25 μm. (c) Mean fluorescent intensity of the HeLa and HEK293 cells obtained from flow cytometry analyses after treatment with DOX-loaded **SNPs** for different time periods in the absence and presence of biotin (*$p < 0.05$). (d) Viability of HeLa and HEK293 cells after incubation with blank **SNPs** for 24 h. Cytotoxicity of (e) HeLa and (f) HEK293 cells with different treatments (*$p < 0.05$). The concentration of **P5-PEG-Biotin⊃PTPE** kept at 200 μg/mL, which was higher than the corresponding CAC value. By changing the ratio between **SNPs** and DOX, DOX-loaded **SNPs** containing different amounts of DOX were prepared.

For the DDSs, multiple biological barriers need to be circumvented when delivering them from the initial site of injection to the sites of action.[20] Poly(ethylene glycol) (PEG), one of the most common non-ionic bioacceptable and nontoxic hydrophilic polymers, has been used in a wide variety of established and emerging applications in pharmaceutics.[21] DDSs coated with PEG shells can prevent themselves from being adsorbed by proteins and decrease the aggregation of the nanovehicles through steric stabilization upon formation of "brush like" shells, which is often utilized to increase the blood circulation time, thus improving the probability that the drug reaches its sites of action before being recognized and internalized by phagocytic cells, and cleared from the body by the reticuloendothelial system (RES). Moreover, DDSs with sizes around 100 nm can be efficiently accumulated in tumor tissues through the leaky tumor vasculature *via* the so-called EPR effect.[22] To determine the pharmacokinetics (pK_a) of DOX-loaded **SNPs**, the plasma concentration of DOX was measured at different time points post injection by using high performance liquid chromatography (HPLC). As shown in Fig. 5a, the blood circulation time of DOX-loaded **SNPs** was much longer than that of free DOX·HCl. Moreover, incorporation of DOX into **SNPs** led to substantially greater area under the curve (AUC) compared to free DOX, confirming that the DOX-loaded **SNPs** possessed a longer blood circulation, thus giving the NPs more opportunity to extravasate from the tumor vessels.

In order to evaluate the drug distribution and accumulation *in vivo*, HeLa tumor bearing Balb/c mice were each injected with free DOX·HCl or DOX-loaded **SNPs** (DOX dosage 5 mg/kg). Fig. 5b shows that DOX was mainly accumulated in the liver and kidneys by formulation of free drug, and only a small amount of DOX appeared in the tumor. On the contrary, formulation with DOX-loaded **SNPs** resulted in remarkably higher accumulation in the tumor (about 3-fold) than the free drug. This improvement should be attributed to the active targeting ability and EPR effect of the DOX-loaded **SNPs**. Quantitative analyses showed that DOX-loaded **SNPs** were inevitably captured by highly perfused organs (lung and liver), which is a common feature for nanoscopic delivery systems,[23] because of the high circulating bloodstream passing through these organs and unavoidable uptake by the RES. It was noteworthy that in most organs including heart, liver, spleen, and kidneys, the magnitude of organ uptake of DOX-loaded **SNPs** was lower than that for free DOX·HCl, indicating that the systemic toxicity towards normal organs was potentially reduced by using **SNPs** as a DDS.

View Article Online
DOI: 10.1039/C6PY01402J

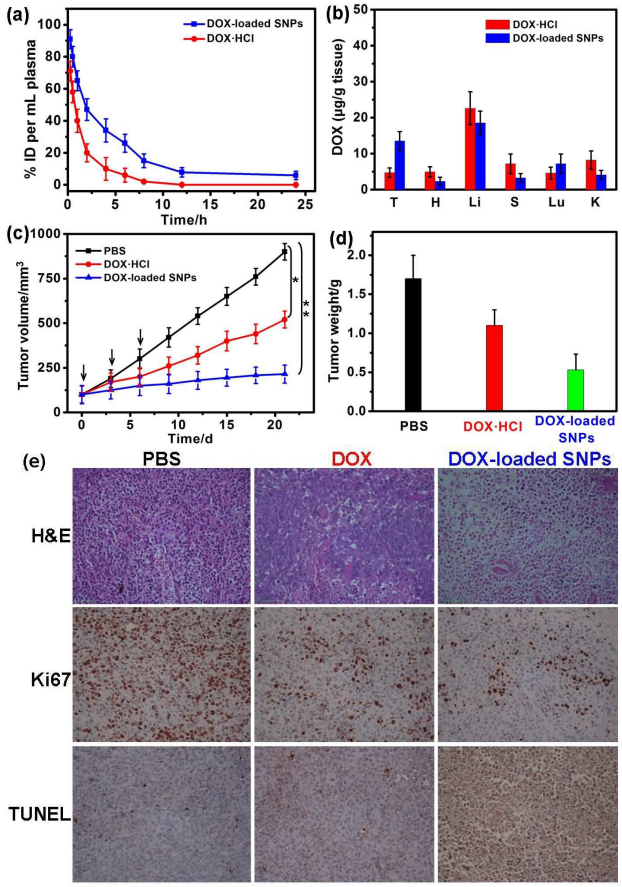

Fig. 5 (a) Blood circulation time of DOX·HCl and DOX-loaded **SNPs** analyzed by measuring plasma concentration of DOX after *i.v.* injection (a dose of 5.00 mg/kg). (b) Tissue distributions of DOX in the main organs at 12 h post-injection. (c) Tumor growth inhibition curves on the HeLa tumor model after various formulations (*p < 0.05, **p < 0.01). (d) The average weight of the tumors of mice bearing HeLa tumors after different treatments. Inset: Photographs of the tumor harvested from the mice after different treatments. (e) H&E, Ki67, and TUNEL analyses of tumor tissues after various formulations.

Ex vivo fluorescence imaging of tumor tissues and major viscera (heart, liver, spleen, lung, and kidneys) revealed no apparent DOX signal in the tumor for the mice receiving free DOX·HCl at 24 h post-injection, because the low-molecular-weight drug was cleared from the body quickly (Fig. S16a). However, the DOX-loaded **SNPs** afforded a superior fluorescence signal in tumours compared with normal organs (Fig. S16b), mainly attributed to their excellent stability in the circulation and higher uptake into the tumour caused by the EPR effect, which was also in good agreement with the results obtained from pK_a and tissue distribution studies. Intratumoral injection of DOX-loaded **SNPs** and free DOX·HCl was also carried out to further demonstrate that the polymeric NPs effectively reside within the tumor. Fig. S17 shows that both formulations display time-dependent *in vivo* fluorescence changes after intratumoral injection. For free DOX·HCl, the red fluorescence signal in the tumor decreased dramatically with time and no apparent DOX signal was detected at 8 h post-injection, suggesting quick clearance of the drug. In the case of DOX-loaded **SNPs**, the fluorescence signal at the tumor site gradually decreased, while relatively high fluorescence was still observed even at 24 h post-injection (Fig. S17), confirming that the DOX-loaded **SNPs** formulation significantly enhanced retention of the drug within the tumor. Theoretically, the red fluorescence signal is quenched when DOX is encapsulated in the DOX-loaded **SNPs** due to the ETR effect. The apperance of the DOX fluorescence signal intumorally indicated the release of the drug, because FRET was blocked, resulting in the recovery of the DOX fluorescence.

To assess the *in vivo* efficacy of DOX-loaded **SNPs** for antitumor treatment, HeLa tumor-bearing mice were exposed to different formulations through intravenous (*i.v.*) injection, including PBS, free DOX·HCl, and DOX-loaded **SNPs**. As shown in Fig. 5c, the inoculated tumors grew fast over time in the group of PBS; the average tumor volume increased from 102 to 912 mm^3 after 21 days. Compared with the PBS control, the mice treated with free DOX·HCl exhibited a moderate tumor inhibition capability. In marked contrast, DOX-loaded **SNPs** exhibited the strongest effect on delaying the tumor growth, with a tumor inhibition rate of 76.7%. Notably, effective tumor inhibition was observed from day 6 post-treatment, by which time only three doses had been injected, suggesting the high effectiveness of the DOX-loaded **SNPs** treatment. Additionally, the images and weights (Fig. 5d) of tumor mass excised after the treatment further confirmed the superior antitumor activity of DOX-loaded **SNPs**. Photos (Fig. 5d and Fig. S19) of resected HeLa tumors from various groups confirmed the much enhanced tumour growth inhibition by DOX-loaded **SNPs** over free DOX·HCl, in accordance with the results discussed above. The above results revealed that the DOX-loaded **SNPs** accumulate in the tumor tissue and perform a sustained release of the encapsulated drug in the acidic tumor environment to inhibit tumor growth.

To evaluate the therapeutic efficacy with different treatments, hematoxylin and eosin (H&E), terminal deoxynucleotidyl transferase dUTP nick end labeling (TUNEL), and Ki67 staining assays were performed to analyze apoptotic cell detection and histological examination of the excised tumor tissues (Fig. 5e). The images of H&E stained tumor tissues presented that both the free DOX·HCl and DOX-loaded **SNPs** treated groups showed varying level of necrosis. Specifically, the DOX-loaded **SNPs** treated group exhibited the most distinct damage to tumor tissues, as lack of discernible boundary regions and much nuclei absence were observed. Compared with PBS or free DOX·HCl, administration of DOX-loaded **SNPs** significantly increased the number of TUNEL-positive tumor cells and reduced the percentage of proliferating Ki67-positive tumor cells, confirming the enhanced efficiency of treatment in inducing apoptosis and inhibiting proliferation in tumor cells.

Systemic toxicity evaluation of the nanocarriers is an crucial parameter for preclinical evaluation. Body weight changes of the mice is an indicator of systemic toxicity. For the mice treated with free DOX·HCl, obvious body weight fluctuation is observed after injection (Fig. S18b), indicating that remarkable side effects were caused by DOX·HCl. In contrast, the DOX-loaded **SNPs** treated group does not display significant body weight fluctuation, indicating that the supramolecular DDS exhibit relatively lower systemic toxicity. Fig. S18a shows the detailed survival rate of

View Article Online
DOI: 10.1039/C6PY01402J

different groups. The mice treated with PBS were all dead during 25 d due to rapid and persistent tumor growth. The survival rate decreased to 28.5% after 1-month treatment for the mice treated with DOX·HCl, because the free anticancer drug may cumulate in health tissue and induce irreversible damage, resulting in severe systemic toxicity. In sharp contrast, the life span of DOX-loaded **SNPs** treated mice obviously was dramatically prolonged, the survival rate reached 85.7 % within 1 month benefiting from the low systemic toxicity and high antitumor efficacy of DOX-loaded **SNPs**.

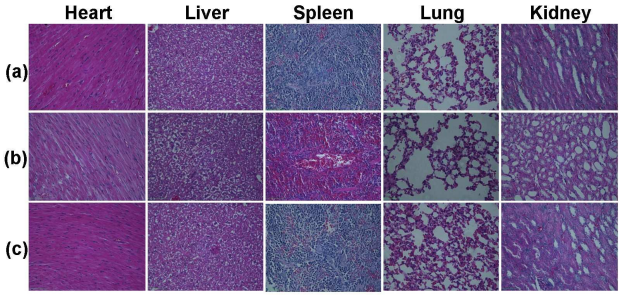

Fig. 6 Histopathologic analysis of major organs after H&E staining, which were harvested from mice treated with (a) PBS, (b) free DOX·HCl, and (c) DOX-loaded **SNPs**.

Histological analysis of major organ slices of the mice treated with free DOX showed severe cardiotoxicity, hepatotoxicity, and nephrotoxicity, which was characterized by notable vacuolization in the cardiomyocytes, prominent steatosis and necrosis in the hepatocytes, and structural disordered renal tubules with pyknotic nuclei and absent lumen (Fig. 6 and Fig. S20). In terms of the **SNPs**-treated group, no obvious tissue lesions could be detected. The low systemic toxicity of **SNPs** was attributed to their long blood circulation, the EPR effect, and the existence of targeting ligands with cancer cell selectivity, which avoided nonspecific uptake by healthy tissues during the circulation. Therefore, undesirable side effects of the anticancer drug were successfully circumvented to minimize the toxicity to healthy tissues by using this supramolecular nanotechnology.

Conclusions

In summary, a novel host–guest molecular recognition motif between a water-soluble pillar[5]arene (**P5**) and a viologen salt (**M**) was established. Based on this novel molecular recognition motif, the first pillar[5]arene-based amphiphilic supramolecular brush copolymer (**P5-PEG-Biotin⊃PTPE**) was constructed, which self-assembled into highly emissive NPs due to the AIE effect. The hydrophobic core of the NPs was utilized to encapsulate anticancer drug DOX, affording a self-imaging DDS. The fluorescence arising from TPE and DOX were both quenched caused by the ETR effect, mediated by FRET and ACQ effect. The "silenced" fluorescence "woke up" after the loaded drug DOX escaped from **SNPs**, which was used to monitor the drug release during delivery process. The biotin ligands decorating on the surfaces of **SNPs** performed as targeting agents to preferentially deliver DOX to biotin receptor over-expressing cancer cells. *In vitro* experiments demonstrated that the efficacy of the drug loaded in **SNPs** was retained, while its cytotoxicity towards normal cell was effectively reduced. *In vivo* investigations showed that the DOX-loaded **SNPs** promoted the antitumor ability with reduced systemic toxicity. The present study provides a novel supramolecular method for the construction of self-imaging DDSs, which have great potential applications in the field of cancer treatment.

Live Subject Statement

Animal care and handling procedures were in agreement with the guidelines evaluated and approved by the ethics committee of Zhejiang University. Study protocols involving animals were approved by the Zhejiang University Animal Care and Use Committee.

Acknowledgements

This work was supported by National Basic Research Program (2013CB834502), the National Natural Science Foundation of China (21434005, 91527301, J1210042), the Fundamental Research Funds for the Central Universities, the Key Science Technology Innovation Team of Zhejiang Province (2013TD02), Open Project of State Key Laboratory of Supramolecular Structure and Materials (sklssm201611), the Intramural Research Program of the National Institute of Biomedical Imaging and Bioengineering, and National Institutes of Health.

Notes and references

1 (a) J. Yuan, Y. Xu, A. Walther, S. Bolisetty, M. Schumacher, H. Schmalz, M. Ballauff and A. H. E. Müller, *Nat. Mater*., 2008, **7**, 718. (b) Y. Chen, A. M. Kushner, G. A. Williams and Z. Guan, *Nat. Chem*., 2012, **4**, 467. (c) M. Krishnamoorthy, S. Hakobyan, M. Ramstedt and J. E. Gautrot, *Chem. Rev*. 2014, **114**, 10976. (d) R. Verduzco, X. Li, S. L. Pesek and G. E. Stein, *Chem. Soc. Rev*., 2015, **44**, 2405.

2 (a) M. A. C. Stuart, W. T. S. Huck, J. Genzer, M. Müller, C. Ober, M. Stamm, G. B. Sukhorukov, I. Szleifer, V. V. Tsukruk, M. Urban, F. Winnik, S. Zauscher, I. Luzinov and S. Minko, *Nat. Mater*., 2010, **9**, 101. (b) G. M. Miyake, R. A. Weitekamp, V. A. Piunova and R. H. Grubbs, *J. Am. Chem. Soc*., 2012, **134**, 14249. (c) B. Li, B. Yu, Q. Ye and F. Zhou, *Acc. Chem. Res.*, 2015, **48**, 229. (d) V. Delplace and J. Nicolas, *Nat. Chem*., 2015, **7**, 771. (e) T. Zhou, H. Qi, L. Han, D. Barbash and C. Y. Li, *Nat. Commun*., 2016, **7**, 11119.

3 (a) H. Gao and K. Matyjaszewski, *J. Am. Chem. Soc*., 2007, **129**, 6633. (b) G. M. Miyake, V. A. Piunova, R. A. Weitekamp and R. H. Grubbs, *Angew. Chem. Int. Ed*., 2012, **51**, 11246. (c) I. Gadwal, J. Rao, J. Baettig and A. Khan, *Macromolecules*, 2014, **47**, 35. (d) J. Ping, Y. Qiao, H. Tian, Z. Shen and X.-H. Fan, *Macromolecules*, 2015, **48**, 592.

4 (a) C. Feng, Y. Li, D. Yang, J. Hu, X. Zhang and X. Huang, *Chem. Soc. Rev*., 2011, **40**, 1282. (b) W. Gu, J. Huh, S. W. Hong, B. R. Sveinbjornsson, C. Park, R. H. Grubbs and T. P. Russell, *ACS Nano*, 2013, **7**, 2551. (c) J. Burdynska, Y. Li, A. V. Aggarwal, S. Hoger, S. S. Sheiko and K. Matyjaszewski, *J. Am. Chem. Soc*., 2014, **136**, 12762.

5 (a) L. Brunsveld, B. J. B. Folmer, E. W. Meijer and R. P. Sijbesma, *Chem. Rev*., 2001, **101**, 4071. (b) F. Huang and H. W. Gibson, *Prog. Polym. Sci*., 2005, **30**, 982. (c) T. F. A. D. Greef, M. M. J. Smulders, M. Wolffs, A. P. H. J. Schenning, R. P. Sijbesma and E. W. Meijer, *Chem. Rev*., 2009, **109**, 5687. (d) L. Fang, M. A. Olson, D. Benítez, E. Tkatchouk, W. A. Goddard III and J. F. Stoddart, *Chem. Soc. Rev*., 2010, **39**, 17. (e) S.-L. Li, T. Xiao, C. Lin and L. Wang, *Chem. Soc. Rev*., 2012, **41**, 5950.

6 (a) X. Yan, F. Wang, B. Zheng and F. Huang, *Chem. Soc. Rev*., 2012, **41**, 6042. (b) P. J. M. Stals, Y. Li, J. Burdynska, R. Nicolay, A. Nese, A. R. A. Palmans, E. W. Meijer, K. Matyjaszewski and S. S. Sheiko, *J. Am. Chem. Soc*., 2013, **135**, 11421. (c) B. V. K. J. Schmidt, M. Hetzer, H. Ritter and C. Barner-Kowollik, *Prog. Polym. Sci*., 2014, **39**, 235. (d) Y. Liu, T. Pauloehrl, S. I. Presolski, L. Albertazzi, A. R. A. Palmans and E. W. Meijer, *J. Am. Chem. Soc*., 2015, **137**, 13096. (e) D.-H. Qu,

View Article Online
DOI: 10.1039/C6PY01402J

Q.-C. Wang, Q.-W. Zhang, X. Ma and H. Tian, *Chem. Rev*., 2015, **115**, 7543.

7 (a) A. K. Bajpai, S. K. Shukla, S. Bhanu and S. Kankane, *Prog. Polym. Sci*., 2008, **33**, 1088. (b) H.-i. Lee, J. Pietrasik, S. S. Sheiko and K. Matyjaszewski, *Prog. Polym. Sci*., 2010, **35**, 24. (c) D. Wang, X. Huan, L. Zhu, J. Liu, F. Qiu, D. Yan and X. Zhu, *RSC Adv*., 2012, **2**, 11953. (d) M. Müllner, S. J. Dodds, T.-H. Nguyen, D. Senyschyn, C. J. H. Porter, B. J. Boyd and F. Caruso, *ACS Nano*, 2015, **9**, 1294.

8 (a) M. Elsabahy and K. L. Wooley, *Chem. Soc. Rev*., 2012, **41**, 2545. (b) S. Mura, J. Nicolas and P. Couvreur, *Nat. Mater*., 2013, **12**, 991.

9 (a) D. A. Leigh, J. K. Y. Wong, F. Dehez and F. Zerbetto, *Nature*, 2003, **424**, 174. (b) A. Fernandes, A. Viterisi, F. Coutrot, S. Potok, D. A. Leigh, V. Aucagne and S. Papot, *Angew. Chem. Int. Ed*., 2009, **48**, 6443. (c) Q. Yan, R. Zhou, C. Fu, H. Zhang, Y. Yin and J. Yuan, *Angew. Chem. Int. Ed*., 2011, **50**, 4923. (d) Q. Yan, Y. Xin, R. Zhou, Y. Yin and J. Yuan, *Chem. Commun*., 2011, **47**, 9594. (e) X. Ji, S. Dong, P. Wei, D. Xia and F. Huang, *Adv. Mater*. 2013, **25**, 5725. (f) Y. Shi, Z. Yang, H. Liu, Z. Li, Y. Tian and F. Wang, *ACS Macro Lett.*, 2015, **4**, 6–10.

10 (a) Q.-C. Wang, D.-H. Qu, J. Ren, K. Chen and H. Tian, *Angew. Chem. Int. Ed.*, 2004, **43**, 2661. (b) Z. Niu and H. W. Gibson, *Chem. Rev*., 2009, **109**, 6024. (c) W. Jiang, A. Schäfer, P. C. Mohr and C. A. Schalley, *J. Am. Chem. Soc.*, 2010, **132**, 2309. (d) Z. Niu, F. Huang and H. W. Gibson, *J. Am. Chem. Soc.*, 2011, **133**, 2836. (e) K. Zhu, V. N. Vukotic and S. J. Loeb, *Angew. Chem. Int. Ed.*, 2012, **51**, 2168. (f) D.-S. Guo and Y. Liu, *Chem. Soc. Rev.*, 2012, **41**, 5907. (g) Y. Lan, X. J. Loh, J. Geng, Z. Walsh and O. A. Scherman, *Chem. Commun*., 2012, **48**, 8757. (h) B. Vinciguerra, L. Cao, J. R. Cannon, P. Y. Zavalij, C. Fenselau and L. Isaacs, *J. Am. Chem. Soc.*, 2012, **134**, 13133. (i) D.-S. Guo, K. Wang, Y.-X. Wang and Y. Liu, *J. Am. Chem. Soc*., 2012, **134**, 10244. (j) S. Erbas-Cakmak, D. A. Leigh, C. T. McTernan and A. L. Nussbaumer, *Chem. Rev.*, 2015, **115**, 10081. (k) R. Barat, T. Legigan, I. Tranoy-Opalinski, B. Renoux, E. Péraudeau, J. Clarhaut, P. Poinot, A. E. Fernandes, V. Aucagne, D. A. Leigh and S. Papot, *Chem. Sci.*, 2015, **6**, 2608.

11 (a) T. Ogoshi, S. Kanai, S. Fujinami, T. A. Yamagishi and Y. Nakamoto, *J. Am. Chem. Soc.*, 2008, **130**, 5022. (b) D. Cao, Y. Kou, J. Liang, Z. Chen, L. Wang and H. Meier, *Angew. Chem. Int. Ed*., 2009, **48**, 9721. (c) M. Xue, Y. Yang, X. Chi, Z. Zhang and F. Huang, *Acc. Chem. Res*., 2012, **45**, 1294. (d) H. Li, D.-X. Chen, Y.-L. Sun, Y. Zheng, L.-L. Tan, P. S. Weiss and Y.-W. Yang, *J. Am. Chem. Soc.,* 2013, **135**, 1570. (e) H. Zhang, X. Ma, K. T. Nguyen and Y. Zhao, *ACS Nano*, 2013, **7**, 7853. (f) C. Li, *Chem. Commun*., 2014, **50**, 12420. (g) W. Si, Z.-T. Li and J.-L. Hou, *Angew. Chem. Int. Ed.,* 2014, **53**, 4578. (h) Z.-Y. Li, Y. Zhang, C.-W. Zhang, L.-J. Chen, C. Wang, H. Tan, Y. Yu, X. Li and H.-B. Yang, *J. Am. Chem. Soc*., 2014, **136**, 8577. (i) N. L. Strutt, H. Zhang, S. T. Schneebeli and J. F. Stoddart, *Acc. Chem. Res.,* 2014, **47**, 2631. (j) Z. Qi, K. Achazi, R. Haag, S. Dong and C. A. Schalley, *Chem. Commun*., 2015, **51**, 10326. (k) T. Ogoshi, S. Takashima and T.-a. Yamagishi, *J. Am. Chem. Soc*., 2015, **137**, 10962. (l) X. Chi, G. Yu, X. Ji, Y. Li, G. Tang and F. Huang, *ACS Macro Lett*., 2015, **4**, 996. (m) Y. Wang, G. Ping and C. Li, *Chem. Commun*., 2016, **52**, 9858.

12 (a) X. Xue, Y. Zhao, L. Dai, X. Zhang, X. Hao, C. Zhang, S. Huo, J. Liu, C. Liu, A. Kumar, W.-Q. Chen, G. Zou and X.-J. Liang, *Adv. Mater*., 2014, **26**, 712. (b) C. Zhang, S. Jin, S. Li, X. Xue, J. Liu, Y. Huang, Y. Jiang, W.-Q. Chen, G. Zou and X.-J. Liang, *ACS Appl. Mater. Interfaces*, 2014, **6**, 5212.

13 (a) X. Xue, S. Jin, C. Zhang, K. Yang, S. Huo, F. Chen, G. Zou and X.-J. Liang, *ACS Nano*, 2015, **9**, 2729. (b) G. Yu, D. Wu, Y. Li, Z. Zhang, L. Shao, J. Zhou, Q. Hu, G. Tang and F. Huang, *Chem. Sci*., 2016, **7**, 3017.

14 (a) C. Li, L. Zhao, J. Li, X. Ding, S. Chen, Q. Zhang, Y. Yu and X. Jia, *Chem. Commun*., 2010, **46**, 9016. (b) G. Yu, C. Han, Z. Zhang, J. Chen, X. Yan, B. Zheng, S. Liu and F. Huang, *J. Am. Chem. Soc*., 2012, **134**, 8711. (c) Q. Duan, Y. Cao, Y. Li, X. Hu, T. Xiao, C. Lin, Y. Pan and L. Wang, *J. Am. Chem. Soc*., 2013, **135**, 10542.

15 (a) J. Luo, Z. Xie, J. W. Y. Lam, L. Cheng, H. Chen, C. Qiu, H. S. Kwok, X. Zhan, Y. Liu, D. Zhu and B. Z. Tang, *Chem. Commun*., 2001, 1740. (b) Y. Hong, J. W. Y. Lam and B. Z. Tang, *Chem. Soc. Rev*., 2011, **40**, 5361. (c) S. Chen, Y. Hong, Y. Liu, J. Liu, C. W. T. Leung, M. Li, R. T. K. Kwok, E. Zhao, J. W. Y. Lam, Y. Yu and B. Z. Tang, *J. Am. Chem. Soc*., 2013, **135**, 4926. (d) J. Geng, K. Li, D. Ding, X. Zhang, W. Qin, J. Liu, B. Z. Tang and Liu, B. *Small*, 2012, **8**, 3655.

16 (a) R. J. Dinis-Oliveira, C. Sousa, F. Remião, J. A. Duarte, A. S. Navarro, M. L. Bastos and F. Carvalho, *Free Radical Bio. Med.*, 2007, **42**, 1017. (b) G. Yu, X. Zhou, Z. Zhang, C. Han, Z. Mao, C. Gao and F. Huang, *J. Am. Chem. Soc*., 2012, **134**, 19489.

17 (a) T. Wei, J. Liu, H. Ma, Q. Cheng, Y. Huang, J. Zhao, S. Huo, X. Xue, Z. Liang and X.-J. Liang, *Nano Lett*., 2013, **13**, 2528. (b) G. Yu, W. Yu, Z. Mao, C. Gao and F. Huang, *Small*, 2015, **11**, 919. (c) K. T. Nguyen and Y. Zhao, *Acc. Chem. Res.*, 2015, **48**, 3016.

18 (a) E. S. Barrett, T. J. Dale and J. Rebek, Jr. *J. Am. Chem. Soc*., 2007, **129**, 8818. (b) B. Prevo and E. J. G. Peterman, *Chem. Soc. Rev*., 2014, **43**, 1144. (c) H. Yuan, J. Qi, C. Xing, H. An, R. Niu, Y. Zhan, Y. Fan, W. Yan, R. Li, B. Wang and S. Wang, *Adv. Funct. Mater*., 2015, **25**, 4412. (d) H.-Q. Peng, L.-Y. Niu, Y.-Z. Chen, L.-Z. Wu, C.-H. Tung and Q.-Z. Yang, *Chem. Rev*., 2015, **115**, 7502.

19 (a) N. Sim and D. Parker, *Chem. Soc. Rev*., 2015, **44**, 2122. (b) Y.-X. Wang, D.-S. Guo, Y.-C. Duan, Y.-J. Wang and Y. Liu, *Sci. Rep*., 2015, **5**, 9019. (c) R. Kumar, W. S. Shin, K. Sunwoo, W. Y. Kim, S. Koo, S. Bhuniya and J. S. Kim, *Chem. Soc. Rev*., 2015, **44**, 6670.

20 (a) R. A. Petros and J. M. DeSimone, *Nat. Rev. Drug Discovery*, 2010, **9**, 615. (b) I. Brigger, C. Dubernet and P. Couvreur, *Adv. Drug Delivery Rev*., 2012, **64**, 24. (c) S. Kunjachan, J. Ehling, G. Storm, F. Kiessling and T. Lammers, *Chem. Rev*., 2015, **115**, 10907. (e) T. Feng, X. Ai, G. An, P. Yang and Y. Zhao, *ACS Nano*, 2016, **10**, 4410.

21 (a) D. Wang, C. Tu, Y. Su, C. Zhang, U. Greiser, X. Zhu, D. Yan and W. Wang, *Chem. Sci*., 2015, **6**, 3775. (b) X. Hu, G. Liu, Y. Li, X. Wang and S. Liu, *J. Am. Chem. Soc.*, 2015, **137**, 362.

22 (a) X. Hu, J. Hu, J. Tian, Z. Ge, G. Zhang, K. Luo and S. Liu, *J. Am. Chem. Soc*., 2013, **135**, 17617. (b) H. J. Kim, H. Takemoto, Y. Yi, M. Zheng, Y. Maeda, H. Chaya, K. Hayashi, P. Mi, F. Pittella, R. J. Christie, K. Toh, Y. Matsumoto, N. Nishiyama, K. Miyata and K. Kataoka, *ACS Nano*, 2014, **8**, 8979. (c) Y. Tian, X. Jiang, X. Chen, Z. Shao and W. Yang, *Adv. Mater*., 2014, **26**, 7393. (d) K. Cai, X. He, Z. Song, Q. Yin, Y. Zhang, F. M. Uckun, C. Jiang and J. Cheng. *J. Am. Chem. Soc.,* 2015, **137**, 3458. (e) J. Song, P. Huang, H. Duan and X. Chen, *Acc. Chem. Res*., 2015, **48**, 2506.

23 (a) X. Duan, J. Xiao, Q. Yin, Z. Zhang, H. Yu, S. Mao and Y. Li, *ACS Nano*, 2013, **7**, 5858. (b) D. Liu, C. Poon, K. Lu, C. He and W. Lin, *Nat. Commun*., 2014, **5**, 4182. (c) Y. Chen, Q. Meng, M. Wu, S. Wang, P. Xu, H. Chen, Y. Li, L. Zhang, L. Wang and J. Shi, *J. Am. Chem. Soc*., 2014, **136**, 16326.

Colour Graphic:

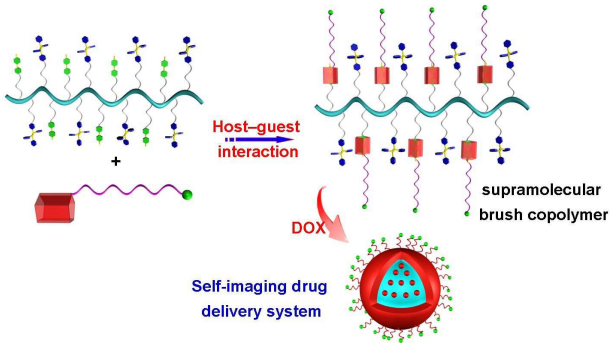

Text:

Here we construct the first pillararene-based amphiphilic supramolecular brush copolymer, which can be utilized as a targeting self-imaging drug delivery vehicle.

View Article Online
DOI: 10.1039/C6PY01402J